PCCP

Accepted Manuscript

ROYAL SOCIETY OF CHEMISTRY

www.rsc.org/pccp

Intrinsic Twisting Instability of Kinked Silicon Nanowires for the Intracellular Recording

Jin-Wu Jiang *

Shanghai Institute of Applied Mathematics and Mechanics,

Shanghai Key Laboratory of Mechanics in Energy Engineering,

Shanghai University, Shanghai 200072, People's Republic of China

Abstract

Kinked silicon nanowire (KSiNW) is a zigzag-shaped nanowire with its growth direction changed regularly at the kinking joints, resulting in a quasi-two-dimensional structure. An intrinsic tendency for the two-dimensional system is to generate some out-of-plane vibrations to withstand the mechanical instability in the third dimension. In the present work, we report the lattice dynamical study for the intrinsic out-of-plane twisting vibration of the KSiNWs. We derive the dynamical matrix analytically, and explore the kinking effect on the phonon spectrum of the KSiNWs. Based on the lattice dynamical analysis, we obtain an analytic formula for the geometrical dependence of the twisting amplitude for the KSiNWs. The analytic formula provides valuable information for the kinking induced twisting stability of KSiNWs serving as bio-probes for the intracellular recording application.

* Correspondence to: jiangjinwu@shu.edu.cn

I. INTRODUCTION

The kinked silicon nanowire (KSiNW) was synthesized by Tian *et al.* in Lieber's group at Harvard University in 2009[1]. Initial efforts have been mainly devoted to investigating the formation of the kinking structure in nanowires from experimental and theoretical communities.[2–16] At present, experimentalists are able to control the growth of kinking structures under different conditions, so more recent works have been mainly focused on practical applications of the KSiNW. It has been demonstrated that the KSiNW is a promising building blocks in bottom-up integration of active devices, taking advantage of its kinking structure. For instance, as a characteristic feature of the KSiNW, the shape of the kinking joint looks like an arrow, so it can act as bio-probes to record intracellular bioelectrical signals.[17,18] A very recent experiment applied the KSiNW to detect the inter and intracellular force during smooth muscle contraction.[19] Considerable progresses have been achieved for this intracellular recording technique based on the free-standing KSiNWs with field-effect transistor enclosed in the arms.[20,21]

In the intracellular recording experiment, the KSiNW serves as the tip end of the detector. During the inserting of the tip end into the celluar, the intrinsic twisting vibration is likely to be actuated due to the kinking configuration of the KSiNW. It is because the joint of the KSiNW will be easily taped by environmental influence, leading to the actuation of twisting motion of the KSiNW. Furthermore, the kinking configuration of the KSiNW is actually a quasi two-dimensional (2D) structure. As we known, an intrinsic tendency of low dimensional structures is to enhance their stability via introducing some movements in the out-of-plane direction, which equivalently increases the dimension. For instance, carbon nanotubes are quasi one-dimensional structures, which can increase their mechanical stability by vibrating in their two lateral directions.[22] As another example, graphene is a quasi 2D system, which is mechanically stable after generating some ripples in the out-of-plane direction.[23] The electrical performance can be affected by the vibration. At finite temperature, phonon density state of each vibration mode follows the Bose-Einstein distribution, if the whole system is at thermal equilibrium state. The electron-phonon interaction thus contributes a constant relaxation time for the electrical properties.[24] However, if the twisting vibration in the kinked silicon nanowire are generated mechanically, then the phonon density state of the twisting mode does not obey the Bose-Einstein distribution anymore.

Consequently, the relaxation time from the electron-phonon interaction is not constant and becomes time dependent; i.e., the twisting vibration induces some turbulence signal in the electrical performance. As a result, the twisting vibration in the KSiNW (if strong enough) will blur the electric signal reading out of the dectector during the intracellular recording. Therefore, the objective of this work is to examine the strength of the intrinsic twisting vibration for the KSiNW.

In this work, we perform a lattice dynamical investigation for KSiNWs, which demonstrates the kinking effect on the phonon spectrum in KSiNWs. The lattice dynamical study helps to examine the intrinsic twisting motion in the direction perpendicular to the KSiNW plane. We obtain an analytic formula for the geometrical dependence of the thermal mean-square vibration amplitude (TMSVA) due to the twisting motion of the KSiNW. It shows that the intrinsic vibration is not strong (with averaged amplitude around 0.46 nm) for KSiNWs used in present experiments, while the analytic formula illustrates that the intrinsic vibration can be considerably strong in KSiNWs with longer arms or thinner cross sections.

II. STRUCTURE AND INTERATOMIC POTENTIAL

The structure of the KSiNW is shown in Fig. 1. The growth direction of the KSiNW changes at the kink, following $< 211 >_{\rm arm}$ to $< 110 >_{\rm joint}$ to $< 211 >_{\rm arm}$, resulting in a quasi 2D configuration with kinking angle $\Theta_0 = 120^\circ$. Two lateral directions are $< 110 >$ and $< 111 >$. The arm length of the KSiNW is L. The thickness of the KSiNW is $W = 80$ nm, and the square cross sectional area is $A = 80nm \times 80nm$.

There are a huge number of silicon atoms in the KSiNW. To accelerate the numerical simulation, we thus introduce the kinked chain model (KCM) to represent the KSiNW structure as shown in Fig. 1 (b). The KCM is a coarse-grained model, and similar chain model has been successfully applied to simulate the mechanical properties of single-walled carbon nanotubes.[25] The chain model has also been implemented to describe lattice dynamical properties of layered structures.[26,27] Each unit cell in the KSiNW is represented by N beads. The bond length (distance between two neighboring beads) for the KCM is b, so we have $L = \frac{N}{2}b$. The mass of the bead in the KCM can be obtained by equaling the total mass of the KCM to the total mass of the KSiNW, i.e., $m_{\rm KCM} = Ab\rho$ with the cross sectional area

A. The silicon mass density $\rho = \frac{8m_{Si}}{a_{Si}^3} = 1.404$ amuÅ^{-3} is taken from bulk silicon with lattice constant $a_{Si} = 5.43$ Å. The whole kinking structure sits in the xy-plane. The Cartesian coordinate system is set as shown in Fig. 1.

We use the valence force field model (VFFM) to calculate the lattice dynamical properties of the KCM. The VFFM has been widely used to compute lattice properties or mechanical properties in covalent materials like diamond,[28] molybdenum disulphide,[29] black phosphorus,[30] silicon,[31] and graphene.[32] According to the specific kinking configuration of the KSiNW, the following four potential terms are adopted to fully describe the lattice dynamical properties of the KCM. See the Method section for more discussions on these VFFM potentials.

The first VFFM term captures the bond stretching between two neighboring beads 1 and 2 in the KCM,

$$V_r = \frac{k_r}{2}\left[(\vec{u}_1 - \vec{u}_2)\cdot\hat{e}_{12}\right]^2, \tag{1}$$

where k_r is the potential parameter. The unit vector $\hat{e}_{12}$ points from bead 1 to 2, while $\vec{u}_j$ is the displacement of bead j.

The second VFFM term describes the bond bending in the left or right arms,

$$V_\theta = \frac{k_\theta}{2}\left(\theta - \theta_0\right)^2, \tag{2}$$

where $\theta_0 = 180°$ is the angle formed by two neighboring bonds, and θ is the angle during vibration.

The third VFFM term corresponds to the bending of the kinking angle at the joint,

$$V_\Theta = \frac{k_\Theta}{2}\left(\Theta - \Theta_0\right)^2, \tag{3}$$

where $\Theta_0 = 120°$ is the initial kinking angle.

The fourth VFFM term is with respect to the twisting of the joint formed by beads 1, 2, and 3, where bead 2 locates at center of the joint of the KCM while beads 1 and 3 are nearby the joint,

$$\begin{aligned} V_{tw} &= \frac{k_{tw}}{2}\left[(\vec{u}_1 - \vec{u}_2)\cdot\hat{e}_z - (\vec{u}_3 - \vec{u}_2)\cdot\hat{e}_z\right]^2 \\ &= \frac{k_{tw}}{2}\left[(\vec{u}_1 - \vec{u}_3)\cdot\hat{e}_z\right]^2, \end{aligned} \tag{4}$$

where $\hat{e}_z$ represents the direction perpendicular to the 2D KCM.

III. DYNAMICAL MATRIX

The lattice dynamical information for the KSiNW are contained in the dynamical matrix, the eigenvalue solution of which provides the frequency and eigen vector of the full phonon spectrum. Hence, an important step is to utilize the above VFFM potential to construct the dynamical matrix, which are obtained analytically in the present work following the equation of motion approach.[33] We consider one unit cell for the KCM, containing N atoms in each arm, so there are totally $2N$ atoms. The atom index is displayed in Fig. 1 (b).

The dynamical matrix from the first VFFM term, V_r, is the following matrix multiplied by the force constant k_r,

$$\begin{pmatrix}
\Phi_L+\Phi_R & -\Phi_L & & & & & & & -\Phi_R\delta_L \\
-\Phi_L & 2\Phi_L & -\Phi_L & & & & & & \\
 & -\Phi_L & \ddots & -\Phi_L & & & & & \\
 & & -\Phi_L & 2\Phi_L & -\Phi_L & & & & \\
 & & & -\Phi_L & \Phi_L+\Phi_R & -\Phi_R & & & \\
 & & & & -\Phi_R & 2\Phi_R & -\Phi_R & & \\
 & & & & & -\Phi_R & \ddots & -\Phi_R & \\
-\Phi_R\delta_R & & & & & & -\Phi_R & 2\Phi_R &
\end{pmatrix}, \tag{5}$$

where the phase factor $\delta_L = e^{-ika}$ and $\delta_R = \delta_L^\star$, with wave vector k and lattice constant $a = 2Nb\sin\frac{\Theta_0}{2}$. The two structural dyads are $\Phi_L = \hat{e}_L\hat{e}_L$ and $\Phi_R = \hat{e}_R\hat{e}_R$, with $\hat{e}_L = \begin{pmatrix} \sin\frac{\Theta_0}{2} & \cos\frac{\Theta_0}{2} & 0 \end{pmatrix}$ as the axial direction for the left arm, and $\hat{e}_R = \begin{pmatrix} -\sin\frac{\Theta_0}{2} & \cos\frac{\Theta_0}{2} & 0 \end{pmatrix}$ as the axial direction for the right arm. These two dyads are related via $\Phi_R = \sigma_x\Phi_L\sigma_x$, in which σ_x is the the reflection symmetry with respect to the yz-plane,

$$\sigma_x = \begin{pmatrix} -1 & 0 & 0 \\ 0 & 1 & 0 \\ 0 & 0 & 1 \end{pmatrix}. \tag{6}$$

The dynamical matrix contributed by the second VFFM term, V_θ, is the following matrix

multiplied by a factor of $\frac{k_\theta}{b^2}$,

$$\begin{pmatrix}
\Psi_L+\Psi_R & -2\Psi_L & \Psi_L & & & & & & & & & & & \Psi_R\delta_L & -2\Psi_R\delta_L \\
-2\Psi_L & 5\Psi_L & -4\Psi_L & \Psi_L & & & & & & & & & & & \\
\Psi_L & -4\Psi_L & 6\Psi_L & -4\Psi_L & \Psi_L & & & & & & & & & & \\
 & \Psi_L & -4\Psi_L & \ddots & \ddots & \Psi_L & & & & & & & & & \\
 & & \Psi_L & \ddots & \ddots & -4\Psi_L & \Psi_L & & & & & & & & \\
 & & & \Psi_L & -4\Psi_L & 6\Psi_L & -4\Psi_L & \Psi_L & & & & & & & \\
 & & & & \Psi_L & -4\Psi_L & 5\Psi_L & -2\Psi_L & & & & & & & \\
 & & & & & \Psi_L & -2\Psi_L & \Psi_L+\Psi_R & -2\Psi_R & \Psi_R & & & & & \\
 & & & & & & & -2\Psi_R & 5\Psi_R & -4\Psi_R & \Psi_R & & & & \\
 & & & & & & & \Psi_R & -4\Psi_R & 6\Psi_R & -4\Psi_R & \Psi_R & & & \\
 & & & & & & & & \Psi_R & -4\Psi_R & \ddots & \ddots & \Psi_R & \\
 & & & & & & & & & \Psi_R & \ddots & \ddots & -4\Psi_R & \Psi_R \\
\Psi_R\delta_R & & & & & & & & & & \Psi_R & -4\Psi_R & 6\Psi_R & -4\Psi_R & \\
-2\Psi_R\delta_R & & & & & & & & & & & \Psi_R & -4\Psi_R & 5\Psi_R &
\end{pmatrix}, \quad (7)$$

where the structural dyads are $\Psi_{L/R} = I - \Phi_{L/R}$ with 3×3 unit matrix I.

The dynamical matrix from the third VFFM term, V_Θ, is the following matrix multiplied by a factor of $\frac{k_\Theta}{b^2 \sin^2 \Theta_0}$,

$$\begin{pmatrix}
(\Omega_R+\Gamma_{RL}+\Gamma_{LR}+\Omega_L) & -(\Omega_R+\Gamma_{LR}) & & & & & & & -(\Gamma_{RL}+\Omega_L)\,\delta_L \\
-(\Omega_R+\Gamma_{RL}) & \Omega_R & & & & & & & \Gamma_{RL}\delta_L \\
 & & \ddots & & & & & & \\
 & & & \Omega_R & -(\Omega_R+\Gamma_{RL}) & \Gamma_{RL} & & & \\
 & & & -(\Omega_R+\Gamma_{LR}) & (\Omega_R+\Gamma_{RL}+\Gamma_{LR}+\Omega_L) & -(\Gamma_{RL}+\Omega_L) & & & \\
 & & & \Gamma_{LR} & -(\Gamma_{LR}+\Omega_L) & \Omega_L & & & \\
 & & & & & & \ddots & & \\
-(\Gamma_{LR}+\Omega_L)\,\delta_R & \Gamma_{LR}\delta_R & & & & & & & \Omega_L
\end{pmatrix}, \quad (8)$$

where the structural dyads are

$$\Omega_L = (\hat{e}_L - \hat{e}_R \cos\Theta_0)(\hat{e}_L - \hat{e}_R \cos\Theta_0); \quad (9)$$

$$\Omega_R = (\hat{e}_R - \hat{e}_L \cos\Theta_0)(\hat{e}_R - \hat{e}_L \cos\Theta_0); \quad (10)$$

$$\Gamma_{LR} = (\hat{e}_L - \hat{e}_R \cos\Theta_0)(\hat{e}_R - \hat{e}_L \cos\Theta_0); \quad (11)$$

$$\Gamma_{RL} = (\hat{e}_R - \hat{e}_L \cos\Theta_0)(\hat{e}_L - \hat{e}_R \cos\Theta_0). \quad (12)$$

A symmetry relationship can be found between Γ_{LR} and Γ_{RL}, i.e., $\Gamma_{LR} = \Gamma_{RL}^\top$.

The dynamical matrix contributed by the fourth VFFM term, V_{tw}, is the following matrix

multiplied by the force constant k_{tw},

$$\begin{pmatrix} 0 & & & & & & 0 \\ & \Xi & & & & & -\Xi\delta_L \\ & & \ddots & & & & \\ & & & \Xi & -\Xi & & \\ & & & & 0 & & \\ & & & -\Xi & \Xi & & \\ & & & & & \ddots & \\ -\Xi\delta_R & & & & & & \Xi \end{pmatrix}, \tag{13}$$

where the structural dyad is $\Xi = \hat{e}_z\hat{e}_z$.

The total dynamical matrix is a summation of the above four dynamical matrix.

IV. VFFM PARAMETERS FOR KSINW

To determine the VFFM parameters for the KCM, we need to compute corresponding mechanical properties of the KSiNWs. All MD simulations for the KSiNW were performed using the publicly available simulation code LAMMPS[34,35], while the OVITO package was used for visualization[36]. The interaction between silicon atoms is described by the Stillinger-Weber potential[37]. Owning to its efficiency and accuracy, this empirical potential has gained a wide application in the simulation of silicon and other similar valence bonded systems. The Newton equations of motion are integrated using the velocity Verlet algorithm with a time step of 1 fs.

The force constant, k_r, for the bond stretching potential in the KCM can be obtained using the Young's modulus of the SiNW. Figure 2 (a) shows the Young's modulus for straight $< 211 >$ SiNWs of different thickness. The two lateral directions of the SiNW are $< \bar{1}11 >$ and $< 01\bar{1} >$. The orientation of the SiNW is in accordance with the arms of the experimental KSiNW samples.[1] All SiNWs and KSiNWs in the present work have square cross section. For SiNWs with thickness $W > 15$ nm, the value of the Young's modulus is almost saturated at 144.1 GPa, which agrees quite well with the Young's modulus in bulk silicon based on first-principal calculations between 110 GPa and 180 GPa.[38–40] The thickness of the experimental KSiNWs are around[1] 80 nm, so their Young's modulus can be approximated to be the saturated value, i.e., 144.1 GPa.

Considering the SiNW is uniaxially deformed by strain ϵ, the total stretching energy within the SiNW is $\frac{1}{2}E\epsilon^2 \times AL$ where A is the cross-sectional area and L is the length of the straight SiNW. The Young's modulus is E. On the other side, if a straight chain model is stretched by strain ϵ, the total strain energy within the chain is $\frac{1}{2}k_r\left(b\epsilon\right)^2 \times N$ where N is the bond number in the chain model satisfying $Nb = L$. From the equaling of the strain energy for both systems, we get the stretching potential parameter for the KCM,

$$k_r \;=\; \frac{EA}{b}. \tag{14}$$

The force constant, k_θ, for the bond bending potential in the KCM can be derived using the bending modulus of the SiNW. To calculate the bending modulus of the SiNW, the SiNW is bent around one lateral direction, i.e., $< \bar{1}11 >$ or $< 01\bar{1} >$, which leads to the same bending modulus value as shown in Fig. 2 (b). We find that the bending modulus of the SiNW is proportional to the square of the thickness. We consider SiNWs of square cross sections, so the bending modulus is actually proportional to the cross sectional area of the SiNW; i.e., $D_\theta = 14.1A$.

For a bending curvature $\kappa = \frac{1}{R}$ for the SiNW, the bending energy is $\frac{1}{2}D_\theta\kappa^2 \times AL$. For the same bending curvature, the chain model is bent by angle $\Delta\theta = b\kappa$. As a result, the bending energy in the chain model is $\frac{k_\theta}{2}\kappa^2 b \times L$. By equaling of the bending energy in the two systems, we get the bond bending parameter k_θ for the KCM,

$$k_\theta \;=\; \frac{D_\theta A}{b} = 14.1\frac{A^2}{b}. \tag{15}$$

The force constant, k_Θ, for the kinking angle bending potential in the KCM can be obtained using the angle bending modulus of the KSiNW. Figure 2 (c) shows that the bending modulus for the kinking angle can be calculated by moving the left and right arms in tangent directions following the arrows in the figure. The obtained angle bending modulus is a function of the cross sectional area, $D_\Theta = 54.5A^2$. For a small variation $\Delta\Theta$ of the kinking angle Θ, the angle bending energy in the KSiNW and the KCM are equaling to each other as,

$$\frac{1}{2}D_\Theta\left(\Delta\Theta\right)^2 \;=\; \frac{1}{2}k_\Theta\left(\Delta\Theta\right)^2, \tag{16}$$

giving the force constant parameter for the bending of the kinking angle, $k_\Theta = D_\Theta = 54.5A^2$.

The force constant, k_{tw}, for the twisting potential in the KCM can be obtained through the twisting modulus of the KSiNW. The twisting modulus of the kinking joint can be

TABLE I: The VFFM parameters for the KCM. The second line lists the geometrical dependence for the VFFM parameters. The third line contains the explicit VFFM parameters for the KCM representing for the KSiNW of cross sectional area $A = 80nm \times 80nm = 6400$ nm^2. The bond length in the KCM is $b = 10a_{Si} = 5.43$ nm.

	b (nm)	m_{KCM} (amu)	$k_r \left(\frac{eV}{nm^2}\right)$	k_θ (eV)	k_Θ (eV)	$k_{tw}\left(\frac{eV}{nm^2}\right)$
expression	$10a_{Si}$	$b \times A \times \frac{8m_{Si}}{a_{Si}^3}$	$\frac{EA}{b}$	$14.1\frac{A^2}{b}$	$54.5A^2$	$\frac{15.5A^{2.5}}{\left(b\cos\frac{\Theta}{2}\right)^2}$
$b = 10a_{Si}$ $A = 6400$ nm^2	5.43	4.88×10^7	1.056×10^6	6.639×10^8	2.233×10^9	3.029×10^8

calculated following the approach shown in Fig. 2 (d). The left and right arms are moved in opposite direction along the out-of-plane direction. The twisting modulus is $\tau = 15.5A^{2.5}$. Equaling the twisting energy in the KCM and KSiNW leads to

$$\frac{1}{2}\tau\left(\Delta\phi\right)^2 = \frac{1}{2}k_{tw}\left(\Delta u_z\right)^2, \tag{17}$$

where the twisting angle is $\Delta\phi = \frac{\Delta u_z}{b\cos\frac{\Theta_0}{2}}$. Hence, the twisting force constant is obtained,

$$k_{tw} = \frac{\tau}{\left(b\cos\frac{\Theta_0}{2}\right)^2} = \frac{15.5A^{2.5}}{\left(b\cos\frac{\Theta_0}{2}\right)^2}. \tag{18}$$

Table I summarizes the expressions for the four VFFM parameters in the KCM. In particular, explicit VFFM parameter values have been provided for KSiNWs of the experimental cross section, i.e., $A = 80nm \times 80nm$.

V. RESULTS AND DISCUSSIONS

A. Phonon spectrum for KSiNWs

Using VFFM parameters listed in Tab. I, we obtain the analytic expression for the full dynamical matrix of KSiNWs by adding up Eqs. (5), (7), (8), and (13); i.e., $D_{\rm tot} = \sum_i D_i$. The eigenvalue solution of the total dynamical matrix leads to the phonon spectrum $\omega(k)$ of the KSiNW, and the eigen vector (vibration morphology) $\mathbf{u}(k,\sigma)$ of each phonon mode (k,σ) as,

$$D_{\rm tot}\mathbf{u}(k,\sigma) = \omega^2(k,\sigma)\mathbf{u}(k,\sigma), \tag{19}$$

where k is the wave vector and σ is the branch index. Fig. 3 shows the four acoustic branches, i.e., the y-direction transverse acoustic (TA_y) branch, the longitudinal acoustic (LA) branch, the twisting (TW) branch, and the z-direction transverse acoustic (TA_z) branch. The full phonon spectrum is shown in the top inset. The lower inset displays the unit cell (by gray rectangular box) with $N = 6$ used for this phonon calculation. The lattice constant is a.

In Fig. 4, we analyze the contribution from each VFFM potential to the four acoustic branches. For instance, in Fig. 4 (a), the frequency $\omega(k, TA_y)$ and the eigen vector $\mathbf{u}(k, TA_y)$ for the TA_y branch has been obtained by Eq. (19). We thus compute the contribution from the i-th VFFM potential by,

$$\omega_i^2(k) = \mathbf{u}^\dagger(k, TA_y) D_i \mathbf{u}(k, TA_y), \tag{20}$$

where $i = 1, 2, 3, 4$ represents for the four dynamical matrix corresponding to V_r, V_θ, V_Θ, and V_{tw}. Insets in each panel display the eigen vector of each phonon mode at wave vector $k = 0.2\pi/a$. The arrow on each atom represents the real component of $\mathbf{u}_j e^{i\Delta_q}$, with phase factor $\Delta_q = k * (qa)$ for the q-th unit cell. Ten unit cells have been used to demonstrate one cycle of the vibration wave with $k = 0.2\pi/a$.

Figure 4 (a) shows that the TA_y branch is dominated by the stretching potential V_r at the Brillouin zone (BZ) boundary, and is mainly contributed by the bond bending potential V_θ in the other BZ region. From its eigen vector shown in the inset, it can be seen that such interplay between the stretching term and bending term is due to the kinking configuration of the KSiNW. Fig. 4 (b) shows that the LA branch is contributed mainly by the stretching potential V_r owning to its stretching-like vibration morphology. The TW branch shown in Fig. 4 (c) and the TA_z branch in Fig. 4 (d) are both dominated by the bond bending potential in the full BZ.

The rest of the paper will be devoted to discussing the two TW modes at the BZ edge ($k = \pi/a$). These two TW modes have the same frequency. Fig. 5 (a) and (b) illustrate the vibration morphology for these two modes of the KSiNW described by the KCM with $N = 50$. The color is with respective to the z component of the eigen vector. In Fig. 5 (a), neighboring joints in the lower regime undergo out-of-phase vibration, while all joints in the upper regime are almost silent. As a result, all joint areas in the upper regime are twisted. For the other TW mode shown in Fig. 5 (b), similar analysis reveals that all joint areas in the lower regime are twisted.

These two TW modes at the BZ edge ($k = \pi/a$) are of particular importance in the KSiNW, because the kinking configuration is actually a quasi 2D structure. A natural tendency of the quasi 2D structure is to enhance its stability by self-actuating vibrations in the out-of-plane direction. For instance, the quasi 2D graphene plane always has vibration induced ripples in the out-of-plane direction, which strengthens its thermal stability.[23] Similarly, these two TW modes generate an out-of-plane vibration for the KSiNW, thus strengthening the thermal stability of the KSiNW. Furthermore, these two TW modes are most easily to be actuated in the KSiNW, due to the kinking configuration. As illustrated by Fig. 5 (c), the arm length of the KSiNW is usually several orders larger than its thickness, so it is easy for an external influence to affect the long arms of the KSiNW. This influence will eventually actuate the TW mode shown in Fig. 5 (a). As a result, these two TW modes generate the most significant effect on the stability of the KSiNW, and is most likely to be detected experimentally.

In Fig. 6, we further examine the eigen vector of the first TW mode shown in Fig. 5 (a) for KSiNW described by the KCM with $N = 50$. Similar results are found for the other TW mode shown in Fig. 5 (b). For a pure twisting motion of the KSiNW around the x-axis for small angle $\delta\omega$, the displacement should be $\vec{u} = \vec{\delta\omega} \times \vec{r} = (\delta\omega)y$. Fig. 6 shows that the z-displacement for the two arms connecting to the same upper joint (at y=145 nm) can be fitted to functions $u_z = 0.4/(e^{-186(y-157)^{-1}-1})$ and $u_z = 0.4/(e^{-173(y-159)^{-1}-1})$. The motion of these two arms are almost out of phase, resulting in the twisting of upper joint regions. For atoms far away from the upper joint, the z-displacement can be approximated to be $u_z \approx 0.002(157 - y)$ and $u_z \approx 0.002(159 - y)$, both of which are linear functions, fulfilling the twisting motion style. However, it is quite interesting that for atoms close to the upper joint region, the z-displacement decays exponentially as $u_z \approx 0.4e^{-186(157-y)}$ or $u_z \approx 0.4e^{-186(159-y)}$. An exponentially decaying eigen vector is a characteristic feature for the localized phonon mode, so it means that the kinking configuration induces some localization effect on the TW mode.

Figure 7 shows the arm length dependence for the frequency of the TW modes. We have comparatively used two different bond lengths; i.e., $b = 5.43$ nm and 10.86 nm. Obviously, the choosing of different bond length value has no effect on the frequency of the TW modes. The frequency is an inverse square function of the arm length. In the above, we have learnt that the TW phonon branch is dominated by the VFFM potential V_θ (see Fig. 4 (c)) and the

corresponding force constant parameter is proportional to the square of the cross-sectional area A, i.e., $k_\theta \propto A^2$ (see Tab. I). The mass of the atom in the KCM is proportional to the cross-sectional area A. As a result, we obtain the geometrical dependence for the TW mode as $\omega = 0.80L^{-2} \times \sqrt{A/(80 \times 80)} = 0.01\sqrt{A}L^{-2}$. We note that the frequency for the TW mode is not dependent on the kink angle Θ_0, because Figure 4 (c) shows that the frequency of the TW mode is dominated by the VFFM potential V_θ which is not related to the kink angle.

B. Twisting vibration analysis

We now examine the averaged vibration amplitude of the TW modes at a given temperature. We derive the TMSVA due to the twisting motion of the KSiNW. Fig. 6 shows that the vibration displacement for the TW mode is a linear function in most regimes, while it decays exponentially nearby the joint that is twisted. The exponential decay illustrates some localized property for the TW mode due to the kinked configuration of the KSiNW. However, the exponential decaying regime is so small that we can approximate the vibration displacement by a linear function, $z\,(y,t) = \xi \frac{y}{L_y} \sin \omega t$ with $L_y = L \cos \frac{\Theta}{2}$ and ξ as the amplitude for the vibration of the joint. This is a general twisting motion of the KSiNW around the axis locating at $y = 0$.

In the bio-probe experiments, only a single kink is used at the tip of the detector, and the two ends of the kink serve as source and drain connections. To be consistent with the experimental set up, we consider only a single kink in the following twisting vibration analysis. The total energy during the twisting vibration in one unit cell is

$$\begin{aligned} E &= \int \frac{1}{2}\rho ds \left(\frac{dz}{dt}\right)^2 + \int \frac{1}{2}\rho ds \omega^2 z^2 \\ &= \frac{1}{2}\left(\frac{1}{3}m\right)\omega^2 \xi^2, \end{aligned} \tag{21}$$

where ds is the length element, and $m = 2L\rho$ is the total mass for one unit cell in the KSiNW described by the KCM. The mass density per length is ρ.

For a particular amplitude ξ, the probability of finding the KSiNW between z and $z + dz$ at (x, y) is $P(\xi, z)dz$. It is proportional to dt. As a result, we have

$$P(\xi, z) \;\propto\; |\frac{dt}{dz}| = \frac{1}{\omega\sqrt{\left(\frac{y}{L_y}\right)^2 \xi^2 - z^2}}. \tag{22}$$

Considering $\int_{-\frac{\xi_y}{L_y}}^{\frac{\xi_y}{L_y}} \frac{1}{\omega\sqrt{\left(\frac{y}{L_y}\right)^2\xi^2-z^2}}dz = \frac{\pi}{\omega}$, we can write down the normalized probability function

$$P(\xi, z) = \frac{1}{\pi\sqrt{\left(\frac{y}{L_y}\right)^2\xi^2 - z^2}}. \tag{23}$$

For the TW mode with frequency ω, the energy of the system is quantized $E_n = (n+\frac{1}{2})\hbar\omega$. The vibration amplitude corresponding to E_n is denoted by ξ_n. The distribution for E_n state at temperature T is given by,

$$\begin{aligned} W_n &= \frac{exp\left[-(n+\frac{1}{2})\hbar\omega/k_BT\right]}{\sum_{p=0}^{+\infty} exp\left[-(p+\frac{1}{2})\hbar\omega/k_BT\right]} \\ &\approx \frac{\hbar\omega}{k_BT}e^{(-n\hbar\omega/k_BT)}, \end{aligned} \tag{24}$$

where the approximation in the last step is applicable for high temperature. This approximation is reasonable for room temperature because the frequency of the TW mode is low.

The thermal averaged probability amplitude is,

$$\begin{aligned} < P(z) > &= \sum_{n=0}^{+\infty} P(\xi_n, z)W_n \\ &= \sum_{n=0}^{+\infty} \frac{1}{\pi\sqrt{\left(\frac{y}{L_y}\right)^2\xi^2 - z^2}} \times \frac{\hbar\omega}{k_BT}e^{(-n\hbar\omega/k_BT)} \\ &= \sqrt{\frac{\frac{1}{6}m\omega^2\left(\frac{L_y}{y}\right)^2}{\pi k_BT}}e^{-\frac{\left(\frac{L_y}{y}\right)^2\frac{1}{6}m\omega^2z^2}{k_BT}}. \end{aligned} \tag{25}$$

This is exactly a Gaussian shaped function $f(x) = \frac{1}{\sqrt{2\pi}}\frac{1}{\sigma}e^{-\frac{(x-\mu)^2}{2\sigma^2}}$. Thus the standard deviation is

$$\sigma^2 = \frac{k_BT}{\frac{1}{3}m\omega^2}\left(\frac{y}{L_y}\right)^2. \tag{26}$$

Obviously, this deviation depends on the y-coordinate, so we do an average for the y-coordinate,

$$\bar{\sigma^2} = \frac{1}{L_y}\int_0^{L_y}\sigma^2 dy = \frac{k_BT}{m\omega^2}. \tag{27}$$

For a KSiNW with arm length L and cross sectional area A, the total mass of one unit cell is $m = 2AL\rho$. The mass density, $\rho = \frac{8m_{Si}}{a_{Si}^3} = 1.404\frac{amu}{\mathring{A}^3}$, is taken from bulk silicon with

lattice constant $a_{Si} = 5.43\mathring{A}$. We have obtained the frequency for the TW mode in the above, i.e., $\omega = 0.01\sqrt{A}L^{-2}$. As a result, we obtain

$$\begin{aligned} \bar{\sigma^2} &= \frac{k_B T}{m\omega^2} = \frac{k_B T}{A2L\rho \times 10^{-4} A L^{-4}} \\ &= 29.38\frac{TL^3}{A^2}. \end{aligned} \tag{28}$$

That is,

$$\frac{\bar{\sigma^2} A^2}{TL^3} = 29.38. \tag{29}$$

The dimensions for quantities in this equation are $[T] = K$, $[L] = \mu m$, $[A] = nm^2$ and $[\bar{\sigma}] = nm$.

For example, at room temperature, the twisting vibration amplitude of a KSiNW of $L = 10\mu m$ and $A = 80nm \times 80nm$ is $\bar{\sigma} = \sqrt{\bar{\sigma^2}} = 0.46$ nm. It indicates that the TMSVA is weak and will probably not influence the sensitivity of the KSiNW based bio-sensor in the experiment. However, Eq. (29) illustrates that the twisting vibration amplitude becomes obviously stronger for thinner or longer KSiNWs, eg. $\bar{\sigma} = 20.8$ nm for KSiNW of length $L = 50\mu m$ and $A = 40nm \times 40nm$. The length of the KSiNW can be manipulated by controling the growing time of the arm in the experiment.[1] Thus, Eq. (29) is able to be validated experimentally for KSiNWs of different size via the TEM set up, which has successfully detected the TMSVA in carbon nanotubes.[22]

VI. CONCLUSION

We have performed lattical dynamical analysis for the phonon spectrum of the KSiNW. We obtain analytic expressions for the dynamical matrix based on the valence force field model, which are used to discuss the kinking effect on the phonon spectrum in KSiNWs. The twisting modes have hybrid linear and exponential eigen vectors, owning to the localization feature of the kinking joints in the KSiNW. Using the lattice dynamical information, we derive an analytic formula for the amplitude of the twisting motion, $\frac{\bar{\sigma}^2 A^2}{TL^3} = 29.38$, disclosing the dependence of the twisting amplitude $\bar{\sigma}$ on the cross-sectional area A and the arm length L at temperature T in the KSiNW.

Acknowledgements

The work is supported by the Recruitment Program of Global Youth Experts of China, the National Natural Science Foundation of China (NSFC) under Grant No. 11504225, and the start-up funding from Shanghai University.

Appendix: Details of the VFFM

We show some key steps in derivation of the bond bending potential expression. Following is another usual VFFM form for the bond bending vibration,

$$V_\theta \;=\; \frac{k_\theta}{2}\left(\cos\theta - \cos\theta_0\right)^2, \tag{30}$$

where θ_0 is the initial bond angle for atoms on the arm in the KCM. For a chain system like the KCM investigated in the present work, we have $\theta_0 = 180^\circ$, leading to

$$\cos\theta - \cos\theta_0 \;\approx\; -\sin\theta_0\left(\Delta\theta\right) - \frac{\cos\theta_0}{2}\left(\Delta\theta\right)^2 = \frac{1}{2}\left(\Delta\theta\right)^2 \propto u^2. \tag{31}$$

As a result, the vibration energy is $V_\theta \propto u^4$, yielding zero dynamical matrix within the linear approximation, so such potential form is not suitable for the derivation of dynamical matrix for a chain system like the KCM.

We have thus described the bond bending using the following potential in the present work,

$$V_\theta \;=\; \frac{k_\theta}{2}\left(\Delta\theta\right)^2. \tag{32}$$

We now demonstrate how to expand this potential in terms of the vibration displacement. Using the Talor expansion in Eq. (31), this bond bending potential takes the form,

$$V_\theta \;=\; k_\theta\left(\cos\theta + 1\right). \tag{33}$$

Let's consider a particular angle θ_{213}. During vibration, the angle is calculated as,

$$\cos\theta \;=\; \frac{\vec{r}_{21}\cdot\vec{r}_{23}}{r_{21}r_{23}}, \tag{34}$$

where $\vec{r}_{21} = \vec{r}_2 - \vec{r}_1$ and $\vec{r}_j = \vec{R}_j + \vec{u}_j$. The initial position for atom j without vibration is $\vec{R}_j$ and the vibration displacement is $\vec{u}_j$. Some algebra lead to,

$$\vec{r}_{21}\cdot\vec{r}_{23} \;=\; -b^2\left(1 + \frac{u^r_{21} + u^r_{23}}{b} - \frac{\vec{u}_{21}\cdot\vec{u}_{23}}{b^2}\right), \tag{35}$$

where $u_{ij}^r = \vec{u}_{ij} \cdot \hat{e}_{ij}^r$ is the projection of vibration displacement on the longitudinal direction, which contributes directly to the change of the bond length, but has no effect on bond angle viration. The distance between two neighboring atoms i and j is $b = R_{ij}$. We also have,

$$r_{21}^{-1} \;=\; b^{-1}\left[1 - \frac{u_{21}^r}{b} - \frac{u_{21}^2}{2b^2} + \frac{3\left(u_{21}^r\right)^2}{2b^2}\right]. \tag{36}$$

Similar expression can be obtained for r_{23}^{-1}. As a result, we get

$$\cos\theta \;=\; -1 + \frac{1}{2b^2}\left(\vec{u}_{21}^{\perp} + \vec{u}_{23}^{\perp}\right)^2, \tag{37}$$

where the displacement vector is decomposed as $\vec{u}_{ij} = u_{ij}^r \hat{e}_{ij}^r + u_{ij}^{\perp}\hat{e}_{ij}^{\perp}$. Finally, the potential in Eq. (32) is expanded in terms of the vibration displacement,

$$V_\theta \;=\; \frac{k_\theta}{2b^2}\left(\vec{u}_{21}^{\perp} + \vec{u}_{23}^{\perp}\right)^2. \tag{38}$$

From the above, we get the angle variation due to vibration, $\Delta\theta = \frac{1}{b}|\vec{u}_{21}^{\perp} + \vec{u}_{23}^{\perp}|$. If both bonds r_{21} and r_{23} are still in the same plane during vibration and assuming $\hat{e}_{21}^{\perp} \cdot \hat{e}_{23}^{\perp} = 1$, we will have $\Delta\theta = \frac{1}{b}\left(u_{21}^{\perp} + u_{23}^{\perp}\right)$ which can be validated geometrically.

[1] B. Tian, P. Xie, T. J. Kempa, D. C. Bell, and C. M. Lieber, Nature Nanotechnology **4**, 824 (2009).

[2] H. Chen, H. Wang, X.-H. Zhang, C.-S. Lee, and S.-T. Lee, Nano Letters **10**, 864 (2010).

[3] S. A. Dayeh, J. Wang, N. Li, J. Y. Huang, A. V. Gin, and S. T. Picraux, Nano Letters **11**, 4200 (2011).

[4] J. H. Kim, S. R. Moon, Y. Kim, Z. G. Chen, J. Zou, D. Y. Choi, H. J. Joyce, Q. Gao, H. H. Tan, and C. Jagadish, Nanotechnology **23**, 115603 (2012).

[5] J. Kim, Y. H. Kim, S.-H. Choi, and W. Lee, ACS Nano **5**, 5242 (2011).

[6] S. Li, X. Zhang, L. Zhang, and M. Gao, Nanotechnology **21**, 435602 (2010).

[7] I. R. Musin and M. A. Filler, Nano Letters **12**, 3363 (2012).

[8] A. Pevzner, Y. Engel, R. Elnathan, A. Tsukernik, Z. Barkay, and F. Patolsky, Nano Letters **12**, 7 (2012).

[9] Y. Qiao, Y. Lin, S. Liu, S. Zhang, H. Chen, Y. Wang, Y. Yan, X. Guo, and J. Huang, Chem Comm **49**, 704706 (2013).

[10] K. W. Schwarz and J. Tersoff, Nano Letters **11**, 316 (2011).

[11] K. W. Schwarz, J. Tersoff, S. Kodambaka, Y.-C. Chou, and F. M. Ross, Physical Review Letters **107**, 265502 (2011).

[12] K. W. Schwarz, J. Tersoff, S. Kodambaka, and F. M. Ross, Physical Review Letters **113**, 055501 (2014).

[13] G. Shen, B. Liang, X. Wang, P.-C. Chen, and C. Zhou, ACS Nano **5**, 2155 (2011).

[14] N. Shin and M. A. Filler, Nano Letters **12**, 2865 (2012).

[15] C. Yan, N. Singh, and P. S. Lee, ACS Nano **4**, 5350 (2010).

[16] T.-T. Zhuang, P. Yu, F.-J. Fan, L. Wu, X.-J. Liu, and S.-H. Yu, Small **10**, 1394 (2014).

[17] Q. Qing, Z. Jiang, L. Xu, R. Gao, L. Mai, and C. M. Lieber, Nature Nanotechnology **9**, 142 (2014).

[18] L. Xu, Z. Jiang, Q. Qing, L. Mai, Q. Zhang, and C. M. Lieber, Nano Letters **13**, 746751 (2013).

[19] J. F. Zimmerman, G. F. Murray, Y. Wang, J. M. Jumper, J. R. Austin, and B. Tian, Nano Letters **DOI:10.1021/acs.nanolett.5b01963** (2015).

[20] L. Xu, Z. Jiang, L. Mai, and Q. Qing, Nano Letters **14**, 3602 (2014).

[21] M. Zhao, B. Cai, Y. Ma, H. Cai, J. Huang, X. Pan, H. He, and Z. Ye, Nanoscale **6**, 4052 (2014).

[22] M. M. J. Treacy, T. W. Ebbesen, and J. M. Gibson, Nature **381**, 678 (1996).

[23] A. Fasolino, J. H. Los, and M. I. Katsnelson, Nature Materials **6**, 858 (2007).

[24] J. T. Lu and J.-S. Wang, Physical Review B **76**, 165418 (2007).

[25] M. J. Buehler, journal of Materials Ressearch **21**, 2855 (2006).

[26] P. H. Tan, W. P. Han, W. J. Zhao, Z. H. Wu, K. Chang, H. Wang, Y. F. Wang, N. Bonini, N. Marzari, N. Pugno, G. Savini, A. Lombardo, and A. C. Ferrari, Nature Materials **11**, 294300 (2012).

[27] Y. Zhao, X. Luo, H. Li, J. Zhang, P. T. Araujo, C. K. Gan, J. Wu, H. Zhang, S. Y. Quek, M. S. Dresselhaus, and Q. Xiong, Nano Letters **13**, 1007 (2013).

[28] M. J. P. Musgrave and J. A. Pople, Proc. R. Soc. (London) Ser. A **268**, 474 (1962).

[29] N. Wakabayashi, H. G. Smith, and R. M. Nicklow, Physical Review B **12**, 659 (1975).

[30] C. Kaneta, H. Katayama-Yoshida, and A. Morita, Solid State Communications **44**, 613 (1982).

[31] S. L. Altmann, A. Lapiccirella, K. W. Lodge, and N. Tomassini, Journal of Physics C: Solid State Physics **15**, 5581 (1982).

[32] T. Aizawa, R. Souda, S. Otani, and Y. Ishizawa, Physical Review B **42**, 11469 (1990).

[33] M. Born and K. Huang, *Dynamical Theory of Crystal Lattices* (Oxford University Press, Oxford, 1954).

[34] Lammps, http://www.cs.sandia.gov/∼sjplimp/lammps.html (2012).

[35] S. J. Plimpton, Journal of Computational Physics **117**, 1 (1995).

[36] A. Stukowski, Modelling and Simulation in Materials Science and Engineering **18**, 015012 (2010).

[37] F. H. Stillinger and T. A. Weber, Physical Review B **31**, 5262 (1985).

[38] K. Y. Kim, R. Sribar, and W. Sachse, Journal of Applied Physics **77**, 5589 (1995).

[39] H. J. McSkimin and P. A. Jr., Journal of Applied Physics **35**, 2161 (1964).

[40] J. J. Wortman and R. A. Evans, Journal of Applied Physics **36**, 153 (1965).

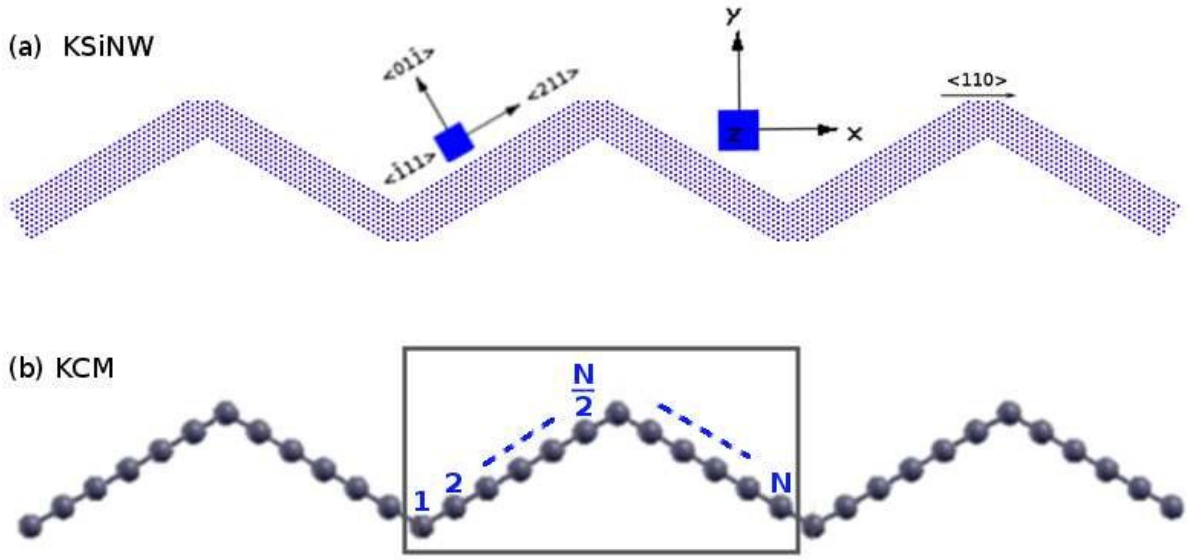

FIG. 1: (Color online) Structure of the KSiNW. (a) The axial direction of the KSiNW changes at the joint, following $< 211 >_{\rm arm}$ to $< 110 >_{\rm joint}$ to $< 211 >_{\rm arm}$. The kinking angle is $\Theta_0 = 120°$. Two lateral directions are $< 110 >$ and $< 111 >$. The arm length is L. (b) The KSiNW is described by the KCM, which is a coarse-grained model with N beads in the arm. The bond length of the KCM is b, satisfying $L = \frac{N}{2}b$.

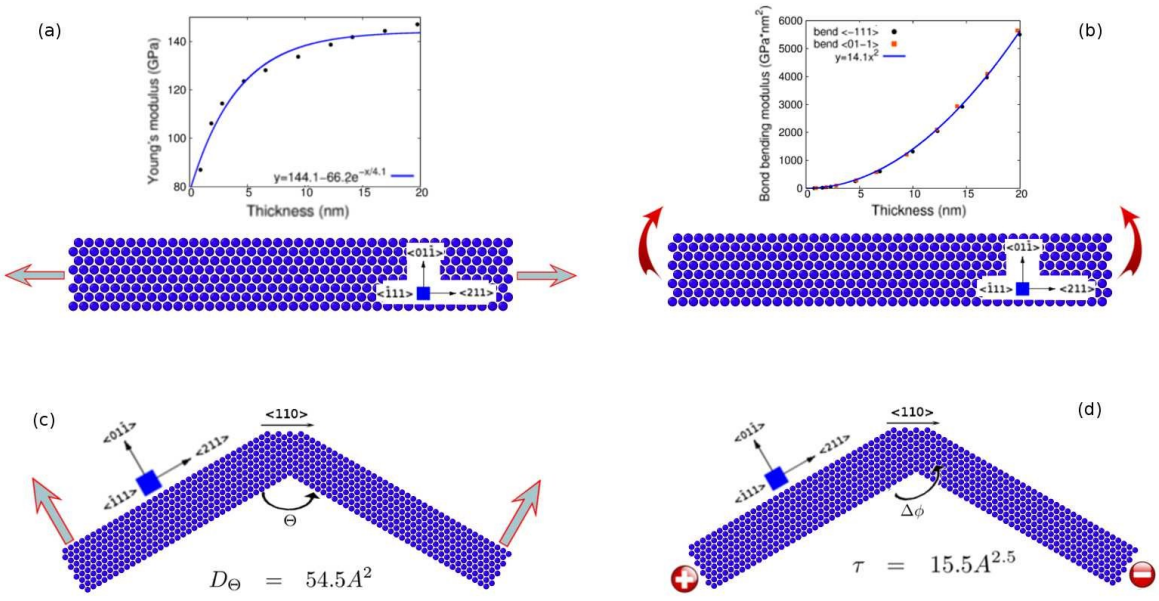

FIG. 2: (Color online) Determining mechanical properties for KSiNWs. (a) Stretching of SiNW. The relationship between the Young's modulus and the thickness W of SiNW is described by $Y = 144.1 - 66.2e^{W/4.1}$. (b) Bending of SiNW. The thickness dependence of the bond bending modulus for SiNW can be fitted to function $D_\theta = 14.1W^2$. (c) Bending of the joint in KSiNW. The angle bending modulus for KSiNW with cross-section A is $D_\Theta = 54.5A^2$. (d) Twisting of the joint in KSiNW. Plus indicates inward direction, and minus means outward direction. The angle twisting modulus for KSiNW with cross-section A is $\tau = 15.5A^{2.5}$.

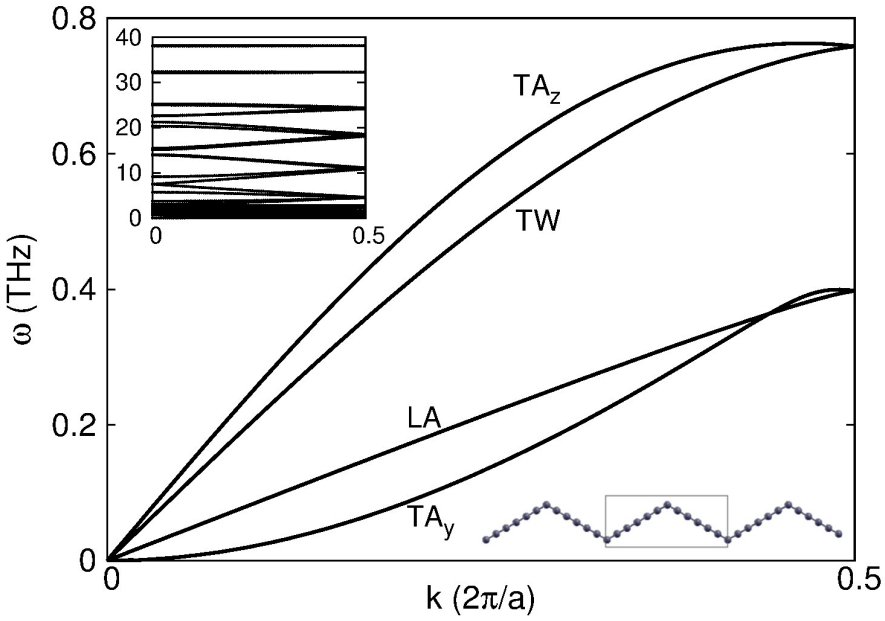

FIG. 3: (Color online) Phonon spectrum for the four acoustic branches in KSiNW described by the KCM with $N = 6$. Force constant parameters are listed in Tab. I. Lower inset displays the unit cell of the KSiNW described by the KCM. Upper inset is the full phonon spectrum.

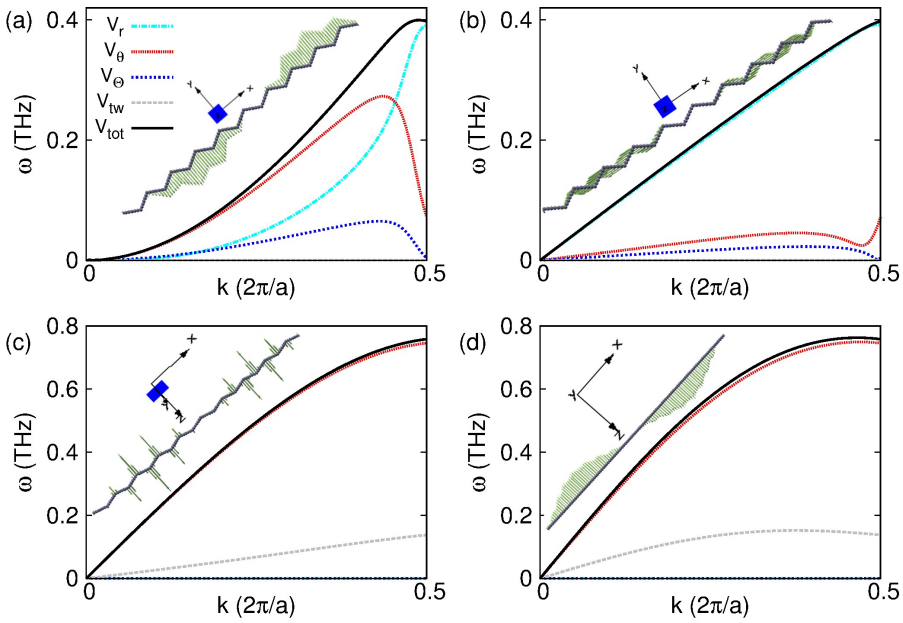

FIG. 4: (Color online) The contribution from each VFFM potential term to the acoustic phonon branches. (a) TA_y branch. (b) LA branch. (c) TW branch. (d) TA_z branch. Insets illustrate the corresponding vibration morphology of the mode at $ka/2\pi = 0.1$ in each branch.

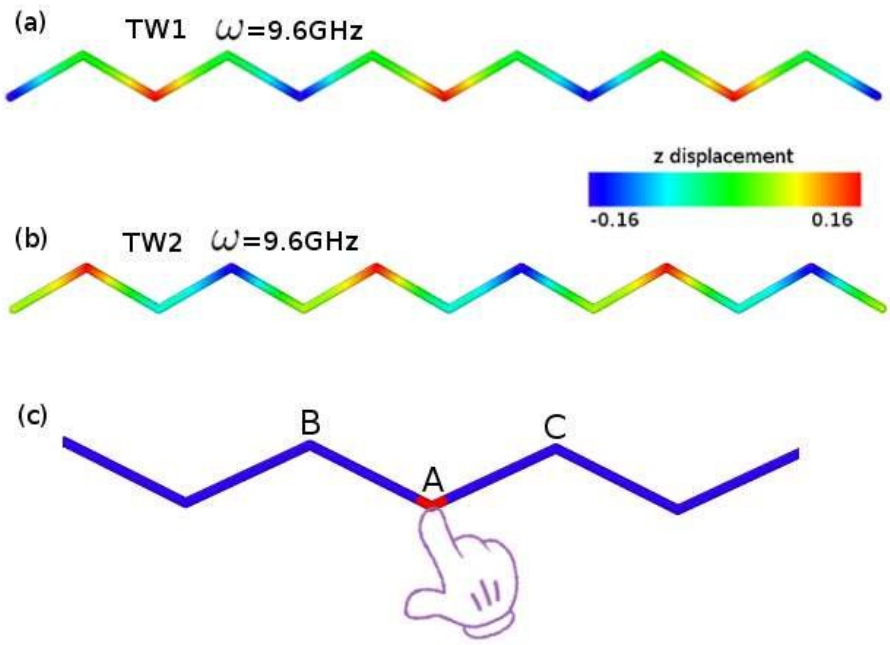

FIG. 5: (Color online) Two twisting mode at $ka/2\pi = 0.5$. Color is with respective to the z-component of the vibration. (a) Neighboring lower joints vibrate in the opposite direction, resulting in the twisting of upper joints. (b) Lower joints are twisted. (c) A schematic diagram demonstrates an easy exactuation of the two twisting modes in (a) and (b). One lower joint 'A' is taped, leading to the twisting of two neighboring upper joints 'B' and 'C', which eventually excites the twisting mode in (a).

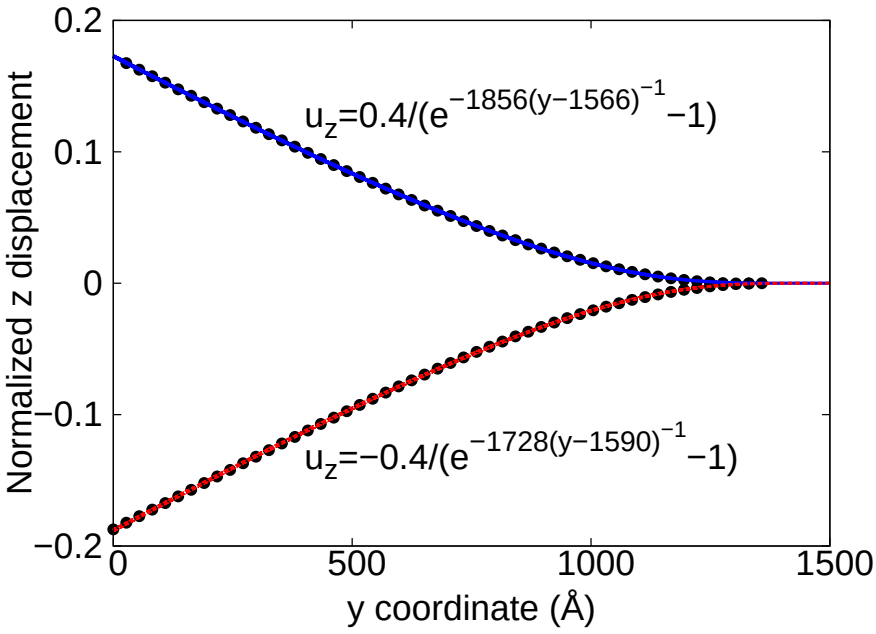

FIG. 6: (Color online) The z-displacement of two neighboring arms (connecting by one upper joint) for the twisting mode in Fig. 5 (a). The upper joint has the maximum y-coordinate of 145 nm.

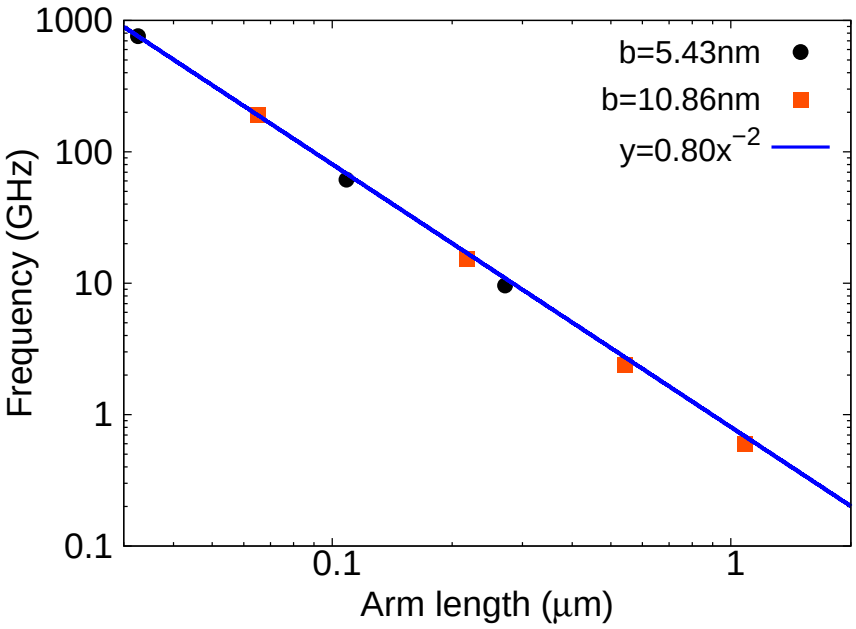

FIG. 7: (Color online) The arm length dependence for frequency of the TW mode in KSiNW with cross-section $80nm \times 80nm$. Data from the KCM with two different bonds 5.43 nm and 10.86 nm fall in the same curve, so the frequency of the TW mode is independent of the choose of the bond length in the KCM.